Journal of Power Sources 273 (2015) 33–40

Contents lists available at ScienceDirect

Journal of Power Sources

journal homepage: www.elsevier.com/locate/jpowsour

Increasing Pt methanol oxidation reaction activity and durability with a titanium molybdenum nitride catalyst support

Yonghao Xiao [a], Zhenggao Fu [a], Guohe Zhan [a], Zhanchang Pan [a, *], Chumin Xiao [a], Shoukun Wu [b], Chun Chen [b], Guanghui Hu [a], Zhigang Wei [a]

[a] School of Chemical Engineering and Light Industry, Guangdong University of Technology, Guangzhou, Guangdong, 510006, China
[b] Huizhou King Brother Electronic Technology Co., Ltd, Huizhou, 516083, China

HIGHLIGHTS

- $Ti_{0.8}Mo_{0.2}N$ with porous structure and high surface area were synthesized.
- $Pt/Ti_{0.8}Mo_{0.2}N$ catalyst exhibits small size and good dispersion of Pt nanoparticles.
- The successful doping of molybdenum element enhanced MOR activity.
- The intrinsic electrochemical stability of the TiN nanostructures was preserved.
- The novel catalyst shows remarkably enhanced MOR activity and durability.

GRAPHICAL ABSTRACT

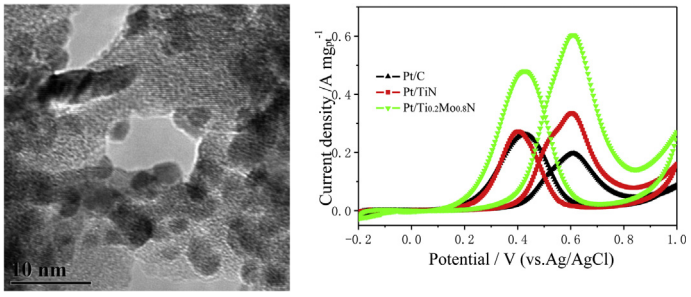

ARTICLE INFO

Article history:
Received 8 July 2014
Received in revised form
5 September 2014
Accepted 8 September 2014
Available online 16 September 2014

Keywords:
Titanium molybdenum nitride
Methanol oxidation reaction
Enhanced stability
Fuel cells

ABSTRACT

Titanium molybdenum nitride ($Ti_{0.8}Mo_{0.2}N$) hybrid support is prepared by a facile and efficient method, including a one-pot solvothermal process followed by a thermal treatment under ammonia at 750 °C, and this hybrid support is further decorated with Pt nanoparticles to catalyze the oxidation of methanol. The catalyst is characterized by X-ray diffraction (XRD), nitrogen adsorption/desorption, transmission electron microscopy (TEM), X-ray photoelectron spectroscopy (XPS) and electrochemical measurements. XRD and TEM results show that the synthesized $Ti_{0.8}Mo_{0.2}N$ is formed as a single-phase solid solution with high purity. Notable, $Ti_{0.8}Mo_{0.2}N$ supported Pt catalyst exhibits a much higher mass activity and durability than that of the conventional Pt/C (E-TEK) electrocatalysts for methanol electrooxidation. The experimental data indicates that the Mo doping has the bifunctional effect that improves the performance and durability of the supported Pt NPs by inducing both co-catalytic and electronic effects.

1. Introduction

Direct methanol fuel cells (DMFCs) is an important portable electric device and power sources due to its high energy conversion efficiency, low operating temperatures, the ease of handling a liquid fuel liquid fuel and compactness [1–6]. However, the large-scale expansion of fuel cell technologies has significantly hindered owing to the high cost, carbon monoxide (CO) poisoning, and insufficient activity and stability [3,7,8]. Furthermore, the widely used carbon-based support can be easily oxidized and converted to carbon dioxide under PEMFC operating conditions, which further

* Corresponding author.
E-mail address: panzhanchang@163.com (Z. Pan).

http://dx.doi.org/10.1016/j.jpowsour.2014.09.057
0378-7753/

results in migration, aggregation, and Ostwald ripening of Pt nanoparticles (NPs), leading to a poor durability for the long-term operations of the fuel cells [9–18]. To address these problems, a number of methods have been proposed, including alloying Pt with secondary transition metals [7,8,19,20] or depositing Pt on the robust no-carbon materials [14,21,22], for developing an electrocatalyst with lower Pt loading, improved performance and durability.

Recently, transition metal nitrides (TMNs) have become a hot topic because of their high conductivity, thermally stable, high corrosion resistance and good catalyst–support interaction [23–25]. The studies show that TiN [22,23], CrN [21], VN [26] and TiNbN [27,28] supported Pt catalysts exhibit enhanced catalytic activity and stability compared with the commercial Pt/C catalyst due to its high conductivity and durability, suggesting that the TMNs have potential as alternative support materials to carbon supports. Specially, many literature reports lay emphasis on TiN NPs not only for its excellent corrosion resistance and electrochemical stability, but also it can act as a co-catalyst that the OH groups can be adsorbed on the TiN surface and help oxidize the poisonous intermediates adhered on adjacent Pt surface, thus the MOR activity was enhanced [25,29]. Additionally, MoN/Mo_2N, which exhibits high Pt-like electrocatalytic activities, has recently attracted extensive attention for applications in fuel cells [30] and Li–O_2 batteries [31,32]. DiSalvo and co-workers [30] found that Mo_2N facilitates the electrooxidation of methanol by activating C–H bond or O–H bond, but raw Mo_2N undergoes redox processes even at a relative low potential (0.75 V Vs.RHE), which is at least somewhat electrochemical unstable for fuel cells uses with a wide range of potential. Based on the above considerations, we are inspired to investigate the electrocatalytic activity of bimetallic titanium molybdenum nitride supported Pt catalyst toward methanol oxidation, since the introduction of Molybdenum element into titanium nitride might improve the electrocatalytic activity of supported Pt catalyst meanwhile the intrinsic electrochemical stability of the TiN nanostructures could be also preserved.

Herein, we present a new approach by exploring a novel support material comprising $Ti_{0.8}Mo_{0.2}N$ to support the Pt NPs. Interestingly, this approach can address the above issues due to the various advantages conferred by the multifunctional $Ti_{0.8}Mo_{0.2}N$ support. The $Ti_{0.8}Mo_{0.2}N$ supported Pt catalyst (Pt/$Ti_{0.8}Mo_{0.2}N$) exhibits high activity and stability for methanol oxidation compared with the commercial Pt/C catalyst (E-TEK). The work demonstrates that $Ti_{0.8}Mo_{0.2}N$ is indeed a promising support to improve Pt catalytic activity and durability for practical catalytic applications.

2. Experimental

2.1. Synthesis of $Ti_{0.8}Mo_{0.2}N$, TiN and MoN NPs

$Ti_{0.8}Mo_{0.2}N$ NPs was prepared using hydrothermal method followed by ammonia annealing treatment. First, $TiMoO_2$ NPs were synthesized by a single-step hydrothermal approach, at a low temperature and without any surfactant or stabilizer. An aqueous solution containing 1.09 g $MoCl_5$ and 3.03 g $TiCl_4$ precursors (the molar ratio, Ti: Mo = 4:1) was prepared and stirred for 30 min, then the mixed solution was transferred to a Teflon-lined autoclave and kept at 150 °C for 3 h. The precipitate was cooled down to the room temperature, followed by filtering, washing thoroughly with deionized water, and then drying in air at 80 °C overnight. Then appropriate amount of the powder precursors was placed in the tubular furnace, annealed at 750 °C under an ammonia gas flow (NH_3, 150 sccm min^{-1})) for 2 h with a progressive heating rate (room temperature to 750 °C, 5 °C min^{-1}). TiN and MoN NPs were prepared in the same processes as $Ti_{0.8}Mo_{0.2}N$ but without the addition of $MoCl_5$ and $TiCl_4$ in the precursors, respectively.

2.2. Synthesis of the catalysts

Pt NPs supported on $Ti_{0.8}Mo_{0.2}N$, TiN and MoN support was prepared by the ethylene glycol (EG) reduction method, and the total Pt loading was controlled ca. 20 wt%. In detail, 80 mg of the support, 60 mg of sodium citrate and 1.33 mL of $H_2PtCl_6 \cdot 6H_2O$ solution (40 mg mL^{-1}) were mixed with 30 mL of EG, followed by vigorous stirring and ultrasonic for 30 min, respectively. Then the mixture was transferred to a flask and heated at 160 °C for 3 h. Subsequently, the suspension was filtered and washed thoroughly with deionized water, and then dried at 80 °C overnight. Commercial Pt/C (E-TEK) catalyst (20 wt% Pt supported on Vulcan XC-72R carbon) was used for comparison.

2.3. Materials characterization

XRD was performed on a Rigaku-Ultima III X-ray diffractometer with Cu Kalpha1 radiation ($\lambda = 1.5405$Å) in the Bragg angle ranging between 20° and 86°. Scanning electron microscopy (SEM) and energy dispersive X-ray analysis (EDX) were conducted with a field-emission scanning electron microscope (FE-SEM, Hitachi S-4800). Transmission electron microscopy (TEM) was performed with a JEOL 2100 microscope. X-ray photoelectron spectroscopy (XPS) was performed on an Axis Ultra DLD X-ray photoelectron spectrometer employing a monochromated Al-Ka X-ray source (hv = 51486.6 eV). Specific surface areas and pore distribution were measured by Brunauer–Emmett–Teller (BET) nitrogen adsorption-desorption on a TristarII 3020 gas adsorption analyzer. The precise Pt loading was measured by inductively coupled plasma optical emission spectrometry (ICP-OES, Leeman PROFILE SPEC) measurements.

2.4. Electrode preparation

A thin film of the electrocatalyst was prepared as follows: 5 mg catalyst was dispersed ultrasonically in 1 mL ethanol for 30 min in ice water bath to form a uniform catalyst ink (1 mg Pt mL^{-1}). A total of 5 μL of well-dispersed catalyst ink was pipetted and spread onto the pre-polished GC electrode. After drying at room temperature, the electrode was then covered by a drop of Nafion solution (0.25 wt% in ethanol solution) and dried in air before measurements. The actual content of Pt was measured by ICP-OES, and the loading amount of Pt for Pt/$Ti_{0.8}Mo_{0.2}N$, Pt/TiN and Pt/C was 25.13, 25.26 and 25.20 μgcm^{-2}, respectively, normalized to the geometric electrode area (0.1964 cm^2).

2.5. Electrochemical measurements

All electrochemical experiments were evaluated on an Autolab electrochemical workstation (Model PGSTAT302N, Metrohm) at room temperature (25 ± 1 °C), using a three-electrode electrochemical cell. The cell consisted of a glassy carbon working electrode (GC electrode, 5 mm inner diameter), an Ag/AgCl (saturated 3 M NaCl) reference electrode, and a platinum foil counter electrode.

Cyclic Voltammetry (CV) characterization of the catalysts in the absence of oxygen was typically carried out in the potential range from 0 to 1.0 V at a scan rate of 50°mVs^{-1} in N_2-saturated 0.5 M H_2SO_4 solution. All of the electrodes were pretreated by cycling the potential between 0 and 1.0 V at a sweep rate of 50 mVs^{-1} for 50 cycles in order to remove any surface contamination prior to MOR activity test. The electrocatalytic properties of the two catalysts toward methanol oxidation were investigated in 1 M

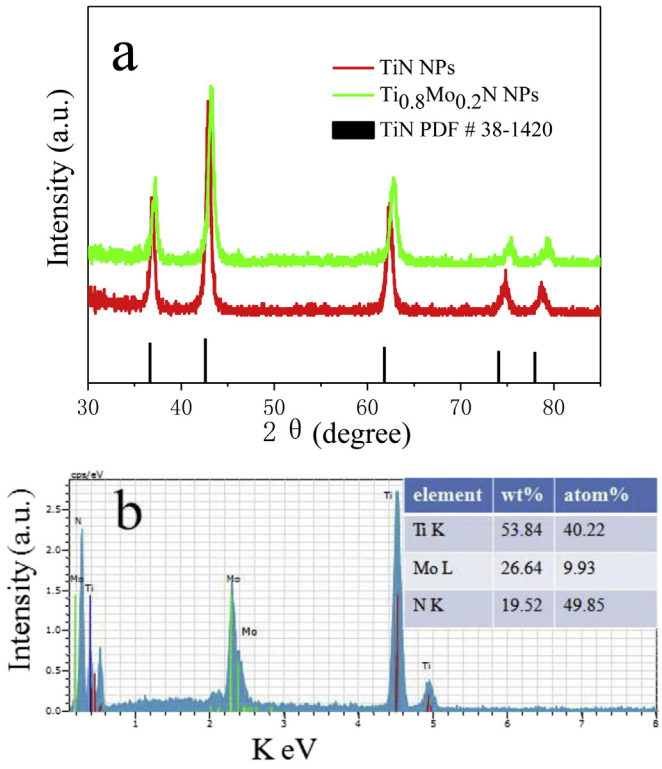

Fig. 1. (a) XRD patterns of prepared TiN and $Ti_{0.8}Mo_{0.2}N$ NPs, (b) EDS profile of $Ti_{0.8}Mo_{0.2}N$ NPs.

CH_3OH + 0.5 M H_2SO_4 solution, and the chronoamperometry curves of Pt/TiN NTs and Pt/C catalyst was held at 0.65 V for various times in 1 M CH_3OH + 0.5 M H_2SO_4 solution.

3. Results and discussion

Fig. 1a compares the XRD patterns of prepared TiN and $Ti_{0.8}Mo_{0.2}N$ NPs. The diffraction peaks of TiN centered at 36.7°, 42.6, 61.8°, 74.1°, and 77.9° that belongs to the face centered cubic (fcc) structure of TiN, and no signal corresponding to impurity peaks were detected, indicating the high purity of the obtained TiN NPs. The diffraction peaks of $Ti_{0.8}Mo_{0.2}N$ was almost identical to that of TiN, and only slightly shifted to higher angles indicated that Mo element was incorporated into the TiN fcc structure to form a single-phase solid solution, for no signals corresponding to a single metallic phase of Mo or to phase separation between titanium and molybdenum nitride was detected. Fig. 1b depicts the EDS profile of $Ti_{0.8}Mo_{0.2}N$, suggesting a Ti:Mo atomic ratio of 40.22:9.93, which is coincide with the atomic ratio of 4:1 used in the precursors. Another four points of the sample was tested by EDS (not shown) and the averaged atomic ratio was 40.31: 9.87. The result implies that the composition of the binary metal nitride can be controlled in a facile manner by adjusting the ratios of $MoCl_5$ and $TiCl_4$ in the precursors.

The TEM and HR-TME images of TiN and $Ti_{0.8}Mo_{0.2}N$ is shown in Fig. 2. Both TiN and $Ti_{0.8}Mo_{0.2}N$ shows a dense solid comprised of fine nanoparticles ca. 10.1 and 8.5, respectively. The good crystallinity of TiN (insert of Fig. 2a) was clearly observed from the well-defined crystalline lattice with a lattice spacing of 0.252 nm, corresponding to the (111) plane of face centered cubic (fcc) TiN [33], which is similar with the lattice spacing of $Ti_{0.8}Mo_{0.2}N$ (Fig. 2b, inset). The above findings were in good agreement with the XRD results, which suggested that $Ti_{0.8}Mo_{0.2}N$ was formed as a single-phase solid solution.

The nitrogen adsorption and desorption isotherm and its corresponding Barrett–Joyner–Halenda (BJH) pore size distribution of TiN and $Ti_{0.8}Mo_{0.2}N$ are shown in Fig. 3a. The BET surface area of the TiN and $Ti_{0.8}Mo_{0.2}N$ NPs are 65 and 148 $m^2\ g^{-1}$, respectively, and both the two supports exhibit a typical type IV isotherm with a distinct hysteretic loop due to the existing of mesopores in the NPs, which can be confirmed by the pore size distribution curve (Fig. 3 b).

Electrochemical stability of TiN and $Ti_{0.8}Mo_{0.2}N$ support was investigated using cyclic voltammetry (CVs) measurement shown in Fig. 4. The samples were tested over a potential range of 0–1.0 V (vs. Ag/AgCl) in a 0.5 M H_2SO_4 solution at room temperature for 50 scans, and no redox currents were observed in their CV traces, which verified the electrochemical stability of TiN and $Ti_{0.8}Mo_{0.2}N$ support (Fig. 4a and b), while MoN is electrochemical unstable and undergoes redox processes even at a relative low potential (Fig. 4c) [30,34]. The above results confirmed the successful doping of molybdenum element into TiN NPs meanwhile the intrinsic electrochemical stability of the TiN nanostructures was preserved.

In order to investigate the particle size distribution of the prepared catalysts, TEM images of Pt/C, Pt/TiN and Pt/$Ti_{0.8}Mo_{0.2}N$ are provided in Fig. 5a–c. The images clearly display that the small, uniformly distributed, darkly contrasting spherical Pt nanoparticles

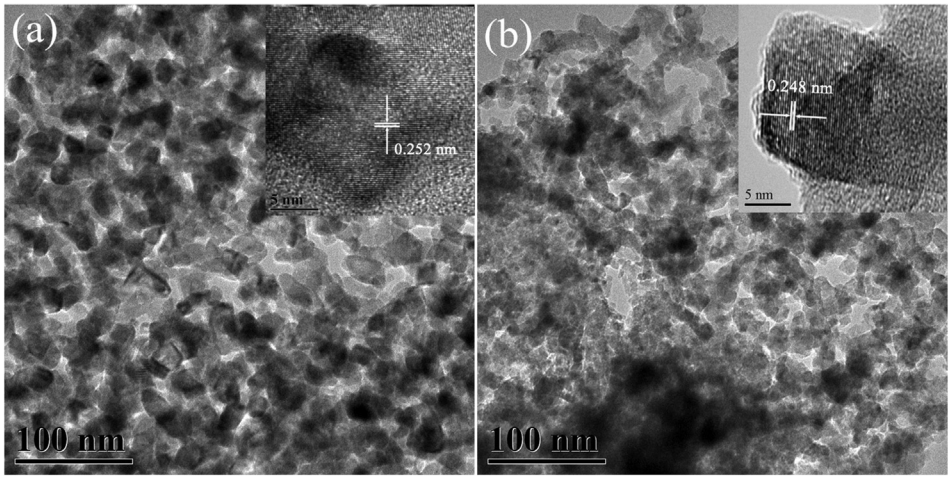

Fig. 2. The TEM images of (a) TiN and (b) $Ti_{0.8}Mo_{0.2}N$ NPs, and insert is the corresponding HR-TEM image.

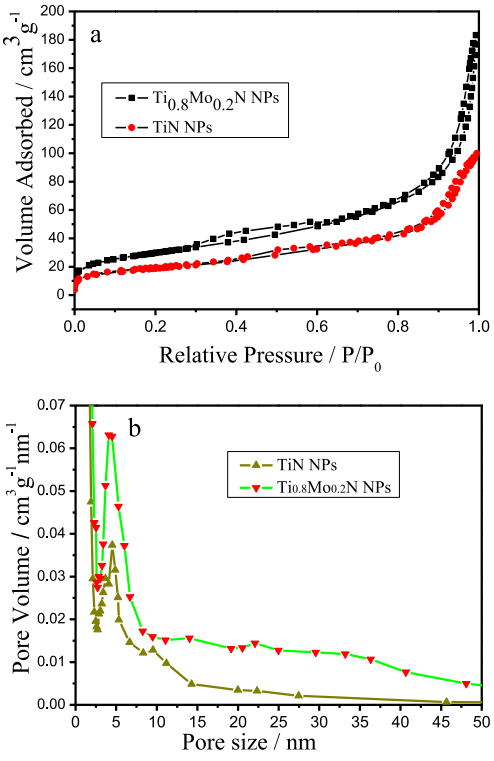

Fig. 3. (a) Nitrogen adsorption/desorption isotherms of TiN and $Ti_{0.8}Mo_{0.2}N$ NPs and (b) its corresponding BJH pore size distribution.

are well anchored on all the three supports. The average size of the particles was calculated from counting the diameter of random 200 Pt nanoparticles of Pt/C, Pt/TiN and Pt/$Ti_{0.8}Mo_{0.2}N$ catalysts is 3.35 ± 0.6, 3.42 ± 0.6 and 3.40 ± 0.4 nm, respectively, with the corresponding histograms, shown in Fig. 5d–f. The difference in averaged Pt particle sizes among the three catalysts was not very large, suggesting that the average Pt particle size was relatively unaffected and the Pt NPs can be highly dispersed on the TiN and $Ti_{0.8}Mo_{0.2}N$ supports as the carbon dose.

Fig. 6 presents the Pt 4f XPS spectra of the Pt/C, Pt/TiN and Pt/$Ti_{0.8}Mo_{0.2}N$ catalysts. Each Pt 4f peak can be deconvoluted into two pairs of doublets. Comparison of the relative areas of integrated intensity of Pt (0) and Pt (II) shows that plentiful Pt exists as Pt (II) in the Pt/C and Pt/TiN catalyst, while only a small amount of Pt (II) is observed in the Pt/$Ti_{0.8}Mo_{0.2}N$, indicating that the introduction of Mo can significantly increase the relative content of Pt (0) in Pt/$Ti_{0.8}Mo_{0.2}N$. In addition, an apparent negative shift of ~0.37 eV in the binding energy of Pt 4f of Pt/$Ti_{0.8}Mo_{0.2}N$, and a positive shift of ~0.23 eV of Pt/TiN catalyst relative to that of the Pt/C catalyst were observed. These results confirmed the strong interaction between Pt and the TiN support, and the electron interactions between Pt and the support was further significant affected by the Mo doping. The negative shift of the Pt 4f binding energy means the Pt NPs can get electrons from the $Ti_{0.8}Mo_{0.2}N$ support [35], leading to a decrease in the d-band vacancy of Pt. As is known, the binary Pt-M alloys is based on electronic transfer mechanisms of the second transition metal (M) to Pt, which modified the surface electronic structure of Pt [36], resulting in a downshift in the d-band center of the surface Pt atoms that the interaction between Pt and absorbed intermediate species was weakened [37–41]. Thus, the adsorbed CO intermediates absorbed on the Pt NPs supported on the $Ti_{0.8}Mo_{0.2}N$ support can be more effectively removed during the MOR process than that of the carbon and TiN supports.

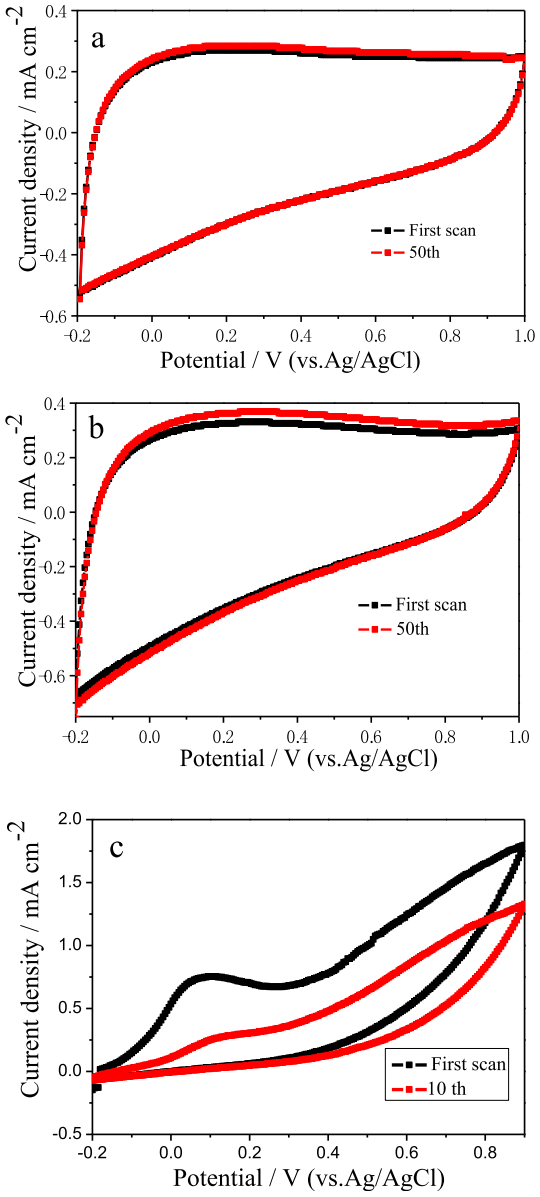

Fig. 4. CV curves of (a) TiN, (b) $Ti_{0.8}Mo_{0.2}N$ and (c) MoN with different cycles over a potential range of 0–1.0 V (vs. Ag/AgCl) in a 0.5 M H_2SO_4 solution at room temperature.

Fig. 7a shows CVs of Pt/C, Pt/TiN and Pt/$Ti_{0.8}Mo_{0.2}N$ catalyst, recorded at room temperature in N_2-purged 0.5 M H_2SO_4 solution at a scan rate of 50 mVs^{-1}. The ECSA ($m^2\ g^{-1}{}_{Pt}$) of the catalysts is estimated according to the equation ECSA = $Q_H/(210 \times W_{Pt})$, where W_{Pt} represents the Pt loading (μgcm^{-2}) on the electrode, Q_H is the total charge (μC) for hydrogen desorption, and 210 represents the charge ($\mu Ccm^{-2}{}_{Pt}$) required to oxidize a monolayer of hydrogen on a clean Pt surface [13,42,43]. The ECSA was measured to be 54.1 and 54.9 m^2g^{-1} for Pt/TiN and Pt/$Ti_{0.8}Mo_{0.2}N$, compared with a 55.4 $m^2\ g^{-1}$ for T-TEK Pt/C catalyst. The similar ECSA of these catalysts were attributed to the same small size and good dispersion of the Pt NPs on the three different supports.

The electrocatalytic properties of Pt/C, Pt/TiN and Pt/$Ti_{0.8}Mo_{0.2}N$ catalysts toward methanol oxidation were investigated in 1 M CH_3OH + 0.5 M H_2SO_4 solution. Fig. 7b shows that the onset potential for Pt/C, Pt/TiN and Pt/$Ti_{0.8}Mo_{0.2}N$ catalyst is 0.38 V, 0.33 V and 0.27 V, clearly indicating that it is more favorable for methanol oxidation on the Pt/TiN and Pt/$Ti_{0.8}Mo_{0.2}N$ catalysts. As shown in

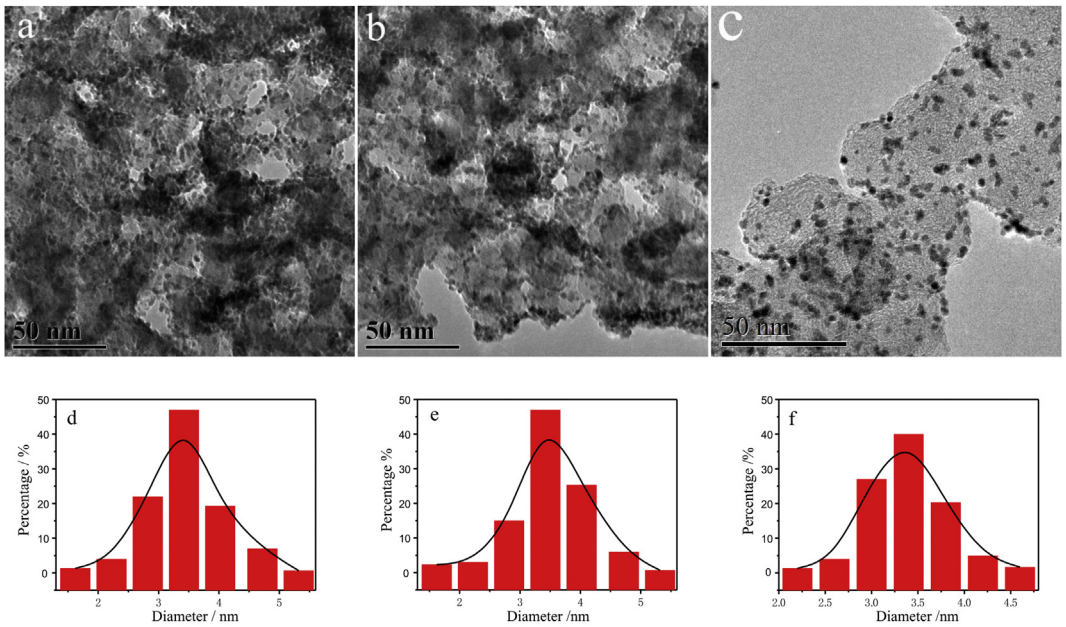

Fig. 5. TEM images of (a) Pt/TiN, (b) Pt/$Ti_{0.8}Mo_{0.2}N$ and (c) Pt/C catalysts, and (d–f) are the corresponding histograms.

Fig. 7b, Pt/$Ti_{0.8}Mo_{0.2}N$ exhibits a mass activity of 611 mAmg^{-1}Pt at 0.6 V, which was about 1.82- and 3.05-fold of that of Pt/TiN and Pt/C catalysts, respectively. Furthermore, the specific activities of the catalysts are also calculated as the current densities normalized to the ECSA of each catalyst. The specific activity of Pt/$Ti_{0.8}Mo_{0.2}N$ is 1.07 mAcm^{-2}, while Pt/TiN and Pt/C are 0.6 and 0.35 mAcm^{-2},

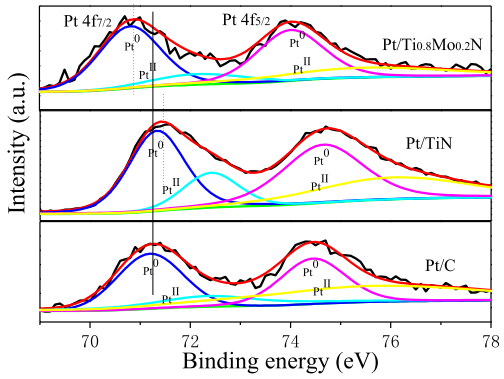

Fig. 6. The Pt 4f XPS spectra of the Pt/C, Pt/TiN and Pt/$Ti_{0.8}Mo_{0.2}N$ catalysts.

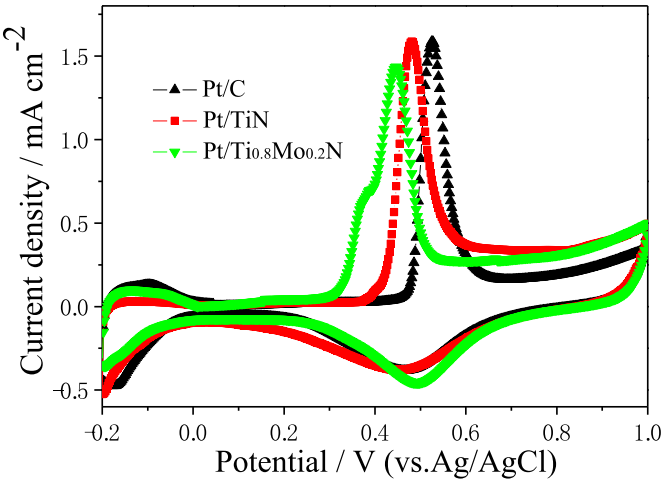

Fig. 8. CO stripping of Pt/C, Pt/TiN and Pt/$Ti_{0.8}Mo_{0.2}N$ catalysts in 0.5 M H_2SO_4 at a scan rate of 50 mVs^{-1} at room temperature.

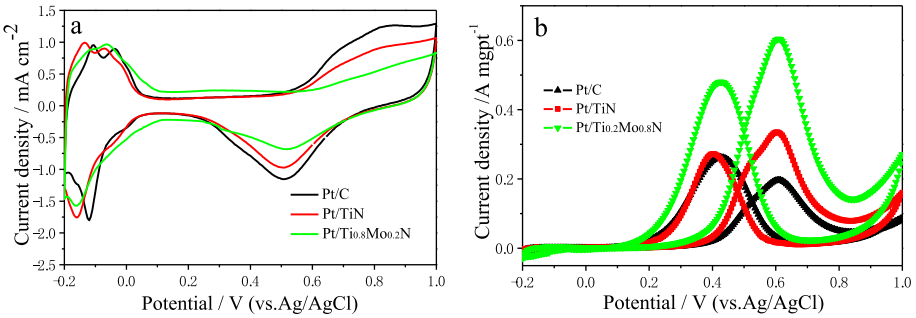

Fig. 7. (a) CVs of Pt/C, Pt/TiN and Pt/$Ti_{0.8}Mo_{0.2}N$ catalyst, recorded at room temperature in N_2-purged 0.5 M H_2SO_4 solution at a scan rate of 50 mVs^{-1}. (b) the mass activities of Pt/C, Pt/TiN and Pt/$Ti_{0.8}Mo_{0.2}N$ catalyst toward the methonal oxidation in 1 M CH_3OH + 0.5 M H_2SO_4 solution.

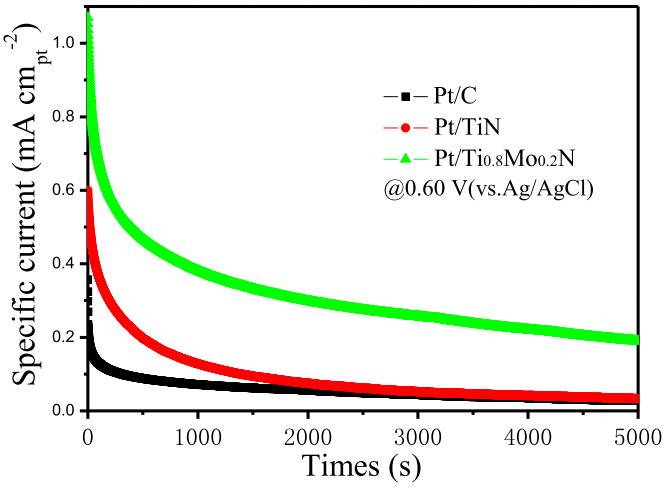

Fig. 9. Chronoamperometry curves of Pt/C, Pt/TiN and Pt/$Ti_{0.8}Mo_{0.2}N$ catalysts held at 0.60 V (vs Ag/AgCl) in 1 M CH_3OH + 0.5 M H_2SO_4 solution for 5000 s.

respectively, indicating that the specific electroactivity of the Pt/$Ti_{0.8}Mo_{0.2}N$ catalyst is obviously higher than that of the Pt/C and Pt/TiN.

To reveal the mechanism of the enhanced activity observed, the electrocatalytic property of the catalysts toward CO oxidation was conducted in 0.5 M H_2SO_4 electrolyte at room temperature. High-purity CO was bubbled into the electrolyte solution for 30 min while keeping the electrode potential at −0.2 V to achieve maximum coverage of CO at the Pt nanoparticles centers. Then the CVs were recorded and shown in Fig. 8. The hydrogen desorption region disappeared in the initial forward scan due to the Pt surface were fully covered by the adsorbed CO. A much larger CO oxidation peak was observed on the Pt/$Ti_{0.8}Mo_{0.2}N$ catalyst, and the onset potentials for CO oxidation of Pt/TiN and Pt/$Ti_{0.8}Mo_{0.2}N$ are 0.37 and 0.29 V, respectively, obviously more negative than that on Pt/C catalyst (0.45 V), demonstrating the facile removal of adsorbed CO intermediates on the Pt/TiN and Pt/$Ti_{0.8}Mo_{0.2}N$ catalysts. A clear shoulder peak in the CO stripping curve in the case of Pt/$Ti_{0.8}Mo_{0.2}N$, and the negative shifted onset potential for CO oxidation compared with Pt/TiN catalyst, which was probably due to the Mo doping. The enhanced CO oxidation of Pt/TiN and Pt/$Ti_{0.8}Mo_{0.2}N$ could be due to the co-catalyst effect that the adsorbed oxygen containing species on the TiN surface [25,29,44], so the oxidation of the CO adhered on the Pt NPs anchored on TiN support can be occurred at a relatively low potential compared with the carbon support. In addition, for Pt/$Ti_{0.8}Mo_{0.2}N$ catalyst, the Mo element doping modifies the surface electronic structure of Pt, introducing a downshift in the d-band center of the surface Pt atoms that resulting in a weakened interaction between Pt NPs and adsorbed CO (detail discussed earlier), further contributing to the facile removal of CO intermediates [40,41]. Furthermore, Mo_2N can facilitate the electrooxidation of methanol by activating C—H bond or O—H bond [30], making it more favorable for methanol oxidation on the Pt/$Ti_{0.8}Mo_{0.2}N$ catalyst. Therefore, Pt/$Ti_{0.8}Mo_{0.2}N$ exhibits higher mass and specific activities towards the MOR than that of the Pt/C and Pt/TiN catalysts.

To further evaluate the rate of surface poisoning, chronoamperometry curves of Pt/C, Pt/TiN and Pt/$Ti_{0.8}Mo_{0.2}N$ catalysts were measured in 1 M CH_3OH + 0.5 M H_2SO_4 solution (Fig. 9). The potential was held at 0.60 V during the measurements. It was clear that the Pt/$Ti_{0.8}Mo_{0.2}N$ catalyst exhibited a slower current degradation over time compared with the Pt/C and Pt/TiN catalysts, indicating a higher tolerance to the poisoning species generated during the MOR process. What's more, a much higher current density was observed for the Pt/$Ti_{0.8}Mo_{0.2}N$ than that of the Pt/C, demonstrating that the Pt/$Ti_{0.8}Mo_{0.2}N$ catalyst was much more electroactive for methanol oxidation. The above results are consistent with the CV results observed in Fig. 7b.

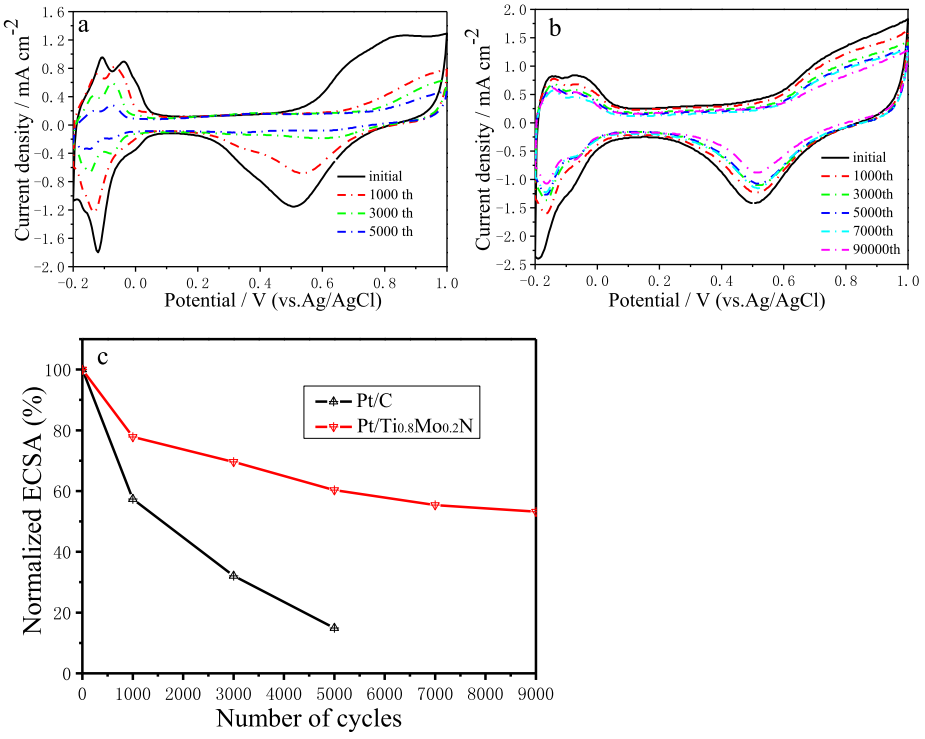

Fig. 10. (a) and (b) show the evolution of CV curves after various cycles for Pt/C and Pt/$Ti_{0.8}Mo_{0.2}N$, respectively. (c) Comparison of ECSA loss for Pt/C and Pt/$Ti_{0.8}Mo_{0.2}N$.

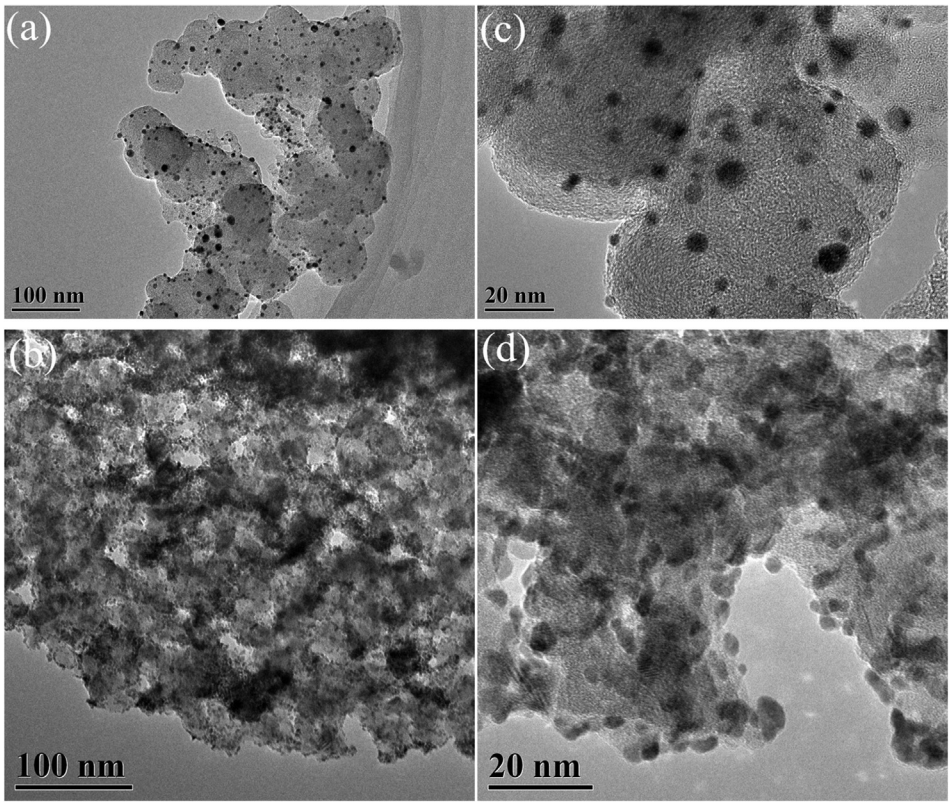

Fig. 11. (a, c) TEM images of collected Pt/C and (b, d) TEM images of collected Pt/$Ti_{0.8}Mo_{0.2}N$ after the ADT test.

The durability of the electrocatalysts remains one of the top issues to be overcome before the widespread application of fuel cells, so the accelerated durability test (ADT) was carried out by cycling the potential between −0.24 and 1.0 V in 0.5 M H_2SO_4 solution at room temperature to test the durability of the catalysts. The evolution of CV curves for Pt/C and Pt/$Ti_{0.8}Mo_{0.2}N$ is shown in Fig. 10. It was clear that Pt/C dropped more than 40% of its initial ECSA after just 1000 cycles, and lost 85% of its initial value after 5000 cycles. However, the Pt/$Ti_{0.8}Mo_{0.2}N$ sample showed great improvement in ECSA loss with 53% remaining even after 9000 cycles. The ADT results confirmed that Pt/$Ti_{0.8}Mo_{0.2}N$ have significantly higher stability than that of the commercial Pt/C catalyst.

To gain further understanding of the enhanced stability observed, the processed Pt/C and Pt/$Ti_{0.8}Mo_{0.2}N$ were collected after 5000 cycles and observed by TEM. As shown in Fig. 11 a and c, the average size of the Pt/C catalyst increases from 3.2 nm to 8.8 nm. Additionally, a significant decrease of Pt density on carbon support was observed after the ADT test, demonstrating that the major cause for ECSA loss of Pt/C was Pt detaching, ripening and the corrosion of the carbon support. However, as for Pt/$Ti_{0.8}Mo_{0.2}N$, the average size of the Pt NPs increases only from 3.2 nm to 4.9 nm and no significant decrease of Pt density on $Ti_{0.8}Mo_{0.2}N$ support was observed. The remaining Pt loading for Pt/C and Pt/$Ti_{0.8}Mo_{0.2}N$ was 17.3% and 7.9%, respectively, revealed by the EDS profile, which was consistent with the TEM results. The TEM and EDS results further confirmed the higher durability of Pt/$Ti_{0.8}Mo_{0.2}N$ compared with the Pt/C catalyst.

4. Conclusions

In summary, we have developed a facile procedure to synthesize Pt/$Ti_{0.8}Mo_{0.2}N$ hybrid catalyst used binary transition metal nitrides, $Ti_{0.8}Mo_{0.2}N$, as the support for Pt, and the experimental results demonstrate that the binary metal nitride can be controlled in a facile manner by adjusting the ratios of precursors. Most importantly, the study data show that Pt/$Ti_{0.8}Mo_{0.2}N$ have a much higher catalytic activity and durability than conventional Pt/C (E-TEK) electrocatalysts for methanol electrooxidation, which is probably due to the synergistic effect introduced by the Mo doping, e.g., inducing both co-catalytic and electronic effects. These advances open up broad possibilities for the design and synthesis of various binary transition metal nitrides as the support for Pt based catalysts with a wide range of applications in energy conversion processes.

Acknowledgments

This research was financially supported by the National Natural Science Foundation of China (20803014), Scientific and technological projects in Guangdong Province (No: 2012B010200035), Huizhou Daya Bay technological projects (20110111) and the 211 funding program of Guangdong Province.

References

[1] L.A. Estudillo-Wong, A.M. Vargas-Gómez, E.M. Arce-Estrada, A. Manzo-Robledo, Electrochimica Acta 112 (2013) 164–170.
[2] S. Meenakshi, K.G. Nishanth, P. Sridhar, S. Pitchumani, Electrochimica Acta 135 (2014) 52–59.
[3] M. Tian, G. Wu, A. Chen, ACS Catal. 2 (2012) 425–432.
[4] T. Maiyalagan, B. Viswanathan, U.V. Varadaraju, J. Nanosci. Nanotechnol. 6 (2006) 2067–2071.
[5] T. Maiyalagan, B. Viswanathan, U.V. Varadaraju, Electrochem. Commun. 7 (2005) 905–912.
[6] P. Strasser, J. Comb. Chem. 10 (2008) 216–224.
[7] V. Bambagioni, C. Bianchini, A. Marchionni, J. Filippi, F. Vizza, J. Teddy, P. Serp, M. Zhiani, J. Power Sources 190 (2009) 241–251.
[8] T. Maiyalagan, Int. J. Hydrogen Energy 34 (2009) 2874–2879.
[9] A. Bauer, K. Lee, C. Song, Y. Xie, J. Zhang, R. Hui, J. Power Sources 195 (2010) 3105–3110.

[10] Y. Shao, G. Yin, Y. Gao, J. Power Sources 171 (2007) 558–566.
[11] S. Sharma, B.G. Pollet, J. Power Sources 208 (2012) 96–119.
[12] D.H. Youn, G. Bae, S. Han, J.Y. Kim, J.-W. Jang, H. Park, S.H. Choi, J.S. Lee, J. Mater. Chem. A 1 (2013) 8007.
[13] B.Y. Xia, N. Wan Theng, H.B. Wu, X. Wang, X.W. Lou, Angew. Chemie-International Ed. 51 (2012) 7213–7216.
[14] H. Van Thi Thanh, K.C. Pillai, H.-L. Chou, C.-J. Pan, J. Rick, W.-N. Su, B.-J. Hwang, J.-F. Lee, H.-S. Sheu, W.-T. Chuang, Energy & Environ. Sci. 4 (2011) 4194–4200.
[15] D.P. He, S.C. Mu, M. Pan, Carbon 49 (2011) 82–88.
[16] V.T. Ho, C.J. Pan, J. Rick, W.N. Su, B.J. Hwang, J. Am. Chem. Soc. 133 (2011) 11716–11724.
[17] R. Kumar, S. Pasupathi, B.G. Pollet, K. Scott, Electrochimica Acta 109 (2013) 365–369.
[18] D. Huang, B. Zhang, J. Bai, Y. Zhang, G. Wittstock, M. Wang, Y. Shen, Electrochimica Acta 130 (2014) 97–103.
[19] S. Zhang, Y. Shao, H.-g. Liao, J. Liu, I.A. Aksay, G. Yin, Y. Lin, Chem. Mater. 23 (2011) 1079–1081.
[20] T. Maiyalagan, J. Solid State Electrochem. 13 (2008) 1561–1566.
[21] M. Yang, R. Guarecuco, F.J. DiSalvo, Chem. Mater. 25 (2013) 1783–1787.
[22] M. Yang, Z. Cui, F.J. DiSalvo, Phys. Chem. Chem. Phys. 15 (2013) 1088–1092.
[23] B. Avasarala, T. Murray, W. Li, P. Haldar, J. Mater. Chem. 19 (2009) 1803.
[24] J. Chen, K. Takanabe, R. Ohnishi, D. Lu, S. Okada, H. Hatasawa, H. Morioka, M. Antonietti, J. Kubota, K. Domen, Chem. Commun. 46 (2010) 7492–7494.
[25] M.M.O. Thotiyl, S. Sampath, Electrochimica Acta 56 (2011) 3549–3554.
[26] M. Yang, Z. Cui, F.J. DiSalvo, Chem. Commun. 48 (2012) 10502.
[27] M. Yang, A.R. Van Wassen, R. Guarecuco, H.D. Abruña, F.J. DiSalvo, Chem. Commun. 49 (2013) 10853.
[28] Z. Cui, R.G. Burns, F.J. DiSalvo, Chem. Mater. 25 (2013) 3782–3784.
[29] M.M.O. Thotiyl, T.R. Kumar, S. Sampath, J. Phys. Chem. C 114 (2010) 17934–17941.
[30] Z. Cui, M. Yang, F.J. DiSalvo, Electrochem. Commun. 33 (2013) 63–67.
[31] K. Zhang, L. Zhang, X. Chen, X. He, X. Wang, S. Dong, L. Gu, Z. Liu, C. Huang, G. Cui, ACS Appl. Mater. Interfaces 5 (2013) 3677–3682.
[32] K. Zhang, L. Zhang, X. Chen, X. He, X. Wang, S. Dong, P. Han, C. Zhang, S. Wang, L. Gu, G. Cui, J. Phys. Chem. C 117 (2013) 858–865.
[33] Y. Dong, Y. Wu, M. Liu, J. Li, ChemSusChem 6 (2013) 2016–2021.
[34] S. Dong, X. Chen, K. Zhang, L. Gu, L. Zhang, X. Zhou, L. Li, Z. Liu, P. Han, H. Xu, J. Yao, C. Zhang, X. Zhang, C. Shang, G. Cui, L. Chen, Chem. Commun. 47 (2011) 11291–11293.
[35] C. Wang, H. Daimon, S.H. Sun, Nano Lett. 9 (2009) 1493–1496.
[36] I. Mintsouli, J. Georgieva, E. Valova, S. Armyanov, A. Kakaroglou, A. Hubin, O. Steenhaut, J. Dille, A. Papaderakis, G. Kokkinidis, S. Sotiropoulos, J. Solid State Electrochem. 17 (2012) 435–443.
[37] V. Stamenkovic, B.S. Mun, K.J.J. Mayrhofer, P.N. Ross, N.M. Markovic, J. Rossmeisl, J. Greeley, J.K. Nørskov, Angew. Chem. 118 (2006) 2963–2967.
[38] J. Suntivich, H.A. Gasteiger, N. Yabuuchi, H. Nakanishi, J.B. Goodenough, Y. Shao-Horn, Nat. Chem. 3 (2011) 546–550.
[39] J. Rossmeisl, P. Ferrin, G.A. Tritsaris, A.U. Nilekar, S. Koh, S.E. Bae, S.R. Brankovic, P. Strasser, M. Mavrikakis, Energy & Environ. Sci. 5 (2012) 8335.
[40] S. Papadimitriou, S. Armyanov, E. Valova, A. Hubin, O. Steenhaut, E. Pavlidou, G. Kokkinidis, S. Sotiropoulos, J. Phys. Chem. C 114 (2010) 5217–5223.
[41] I. Mintsouli, J. Georgieva, S. Armyanov, E. Valova, G. Avdeev, A. Hubin, O. Steenhaut, J. Dille, D. Tsiplakides, S. Balomenou, S. Sotiropoulos, Appl. Catal. B: Environ. 136–137 (2013) 160–167.
[42] S. Guo, S. Dong, E. Wang, Acs Nano 4 (2010) 547–555.
[43] L.X. Ding, A.L. Wang, G.R. Li, Z.Q. Liu, W.X. Zhao, C.Y. Su, Y.X. Tong, J. Am. Chem. Soc. 134 (2012) 5730–5733.
[44] M.M. Ottakam Thotiyl, T. Ravikumar, S. Sampath, J. Mater. Chem. 20 (2010) 10643.